Supplemental Information

Phenotypic Signature of Circulating Neoantigen-Reactive CD8$^+$ T cells From Metastatic Human Cancers

Rami Yossef[1]†*, Sri Krishna[1]†*, Sivasish Sindiri[1], Frank J. Lowery[1], Amy R. Copeland[1], Jared J. Gartner[1], Maria R. Parkhurst[1], Neilesh B. Parikh[1], Kyle J. Hitscherich[1], Shoshana T. Levi[1], Praveen D. Chatani[1], Nikolaos Zacharakis[1], Noam Levin[1], Nolan R. Vale[1], Shirley K. Nah[1], Aaron Dinerman[1], Victoria K. Hill[1], Satyajit Ray[1], Alakesh Bera[1], Lior Levy[1], Li Jia[2], Michael C. Kelly[3], Stephanie L. Goff[1], Paul F. Robbins[1], Steven A. Rosenberg[1]*

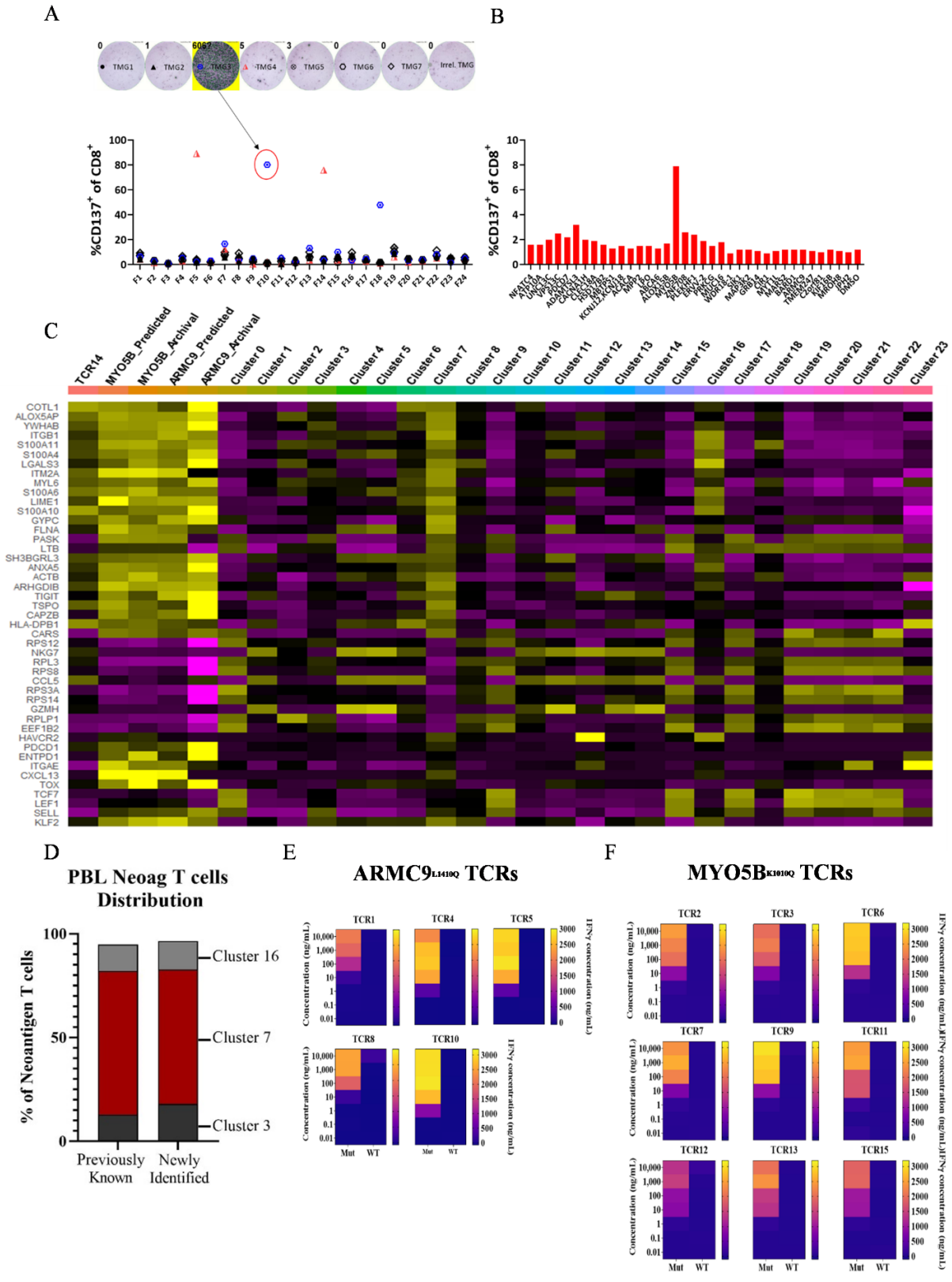

Supplemental Figure S1: Neoantigen-specific TIL reactivity screen against patient's 4246 tumoral mutations, and phenotype, distribution, and specificity of neoantigen-specific TCRs in PBL of Pt.4246, related to Figure 1.

(A) CD137 upregulation on *in vitro* expanded TIL, grown from tumor fragments, following co-cultured with autologous DCs electroporated with TMGs encoding for patient's tumoral mutations. Inset: an example of interferon-gamma (IFNγ) secretion from TIL fragment 10 (F10) following the co-culture. **(B)** Upregulation of CD137 on fragment 10 TILs following co-culture with autologous APCs pulsed with mutated peptides encoded by TMG3. **(C)** Gene expression heatmap showing top 25 upregulated and 10 downregulated genes in neoantigen-reactive cells, and the last 10 rows represent genes-of-interest. **(D)** Frequency of neoantigen-reactive T cell clones (n = 18) in clusters 3, 7, and 16. (**E-F)** IFNγ secretion following overnight co-culture of 14 candidate TCRs transduced into healthy donor PBL predicted from cluster 7 with imDCs pulsed with titrated concentrations of mutated neoantigenic epitope and their wildtype counterparts for ARMC9 (**E)** or MYO5B **(F)** or their wild-type counterpart.

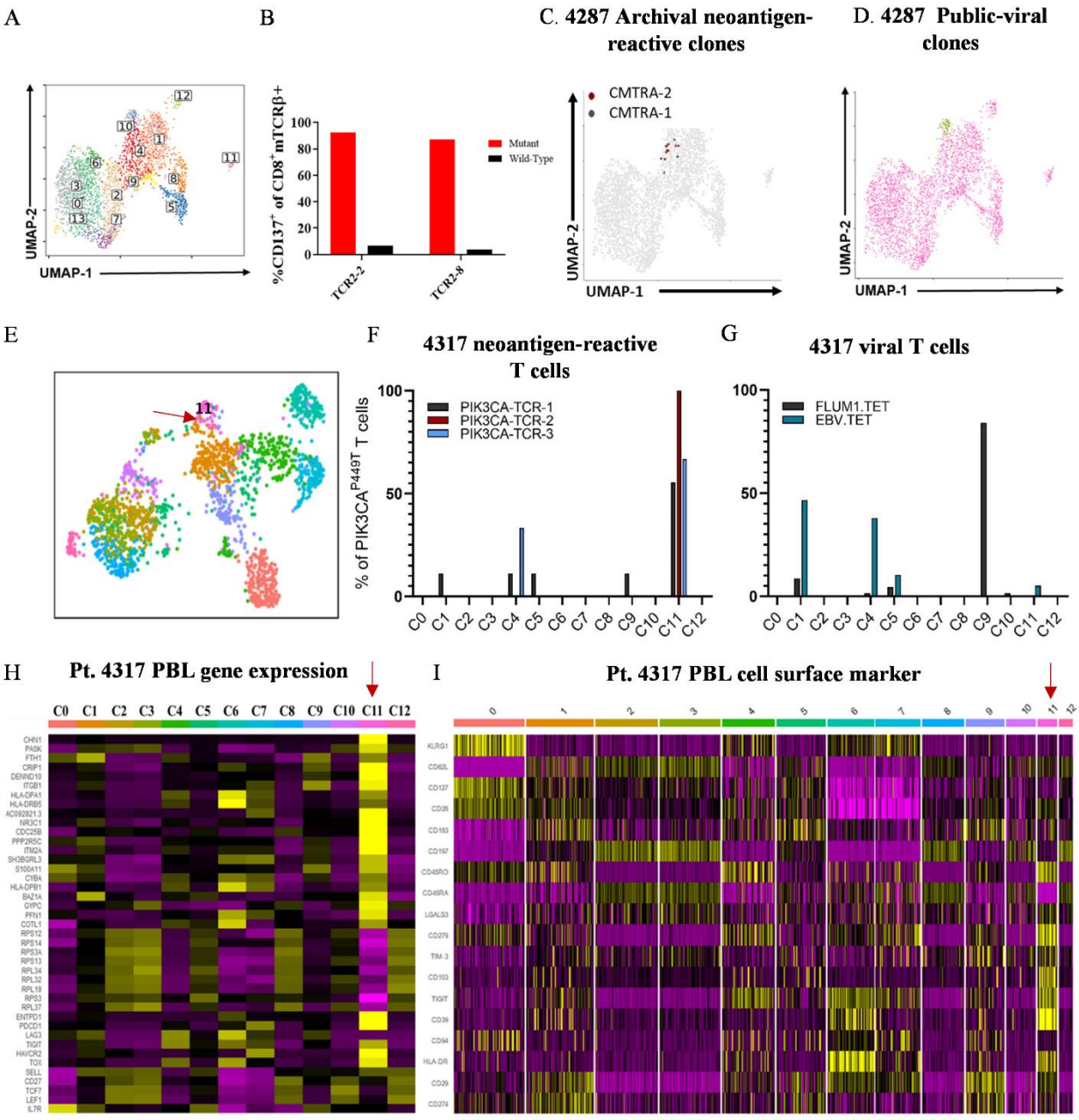

Supplemental Figure S2: Phenotypic clustering of Pt. 4287and Pt. 4317 tetramer-enriched circulating CD8⁺ PBLs, related to Figure 1 (A) UMAP transcriptome clustering CMTR1^{K601T} tetramer enriched cells (1500 CMTR1 ^{K601T}:HLA-B*49 tetramer^{pos} cells spiked into a total of 40,000 CD8 cells). **(B)** TCR-transduced PBLs were co-cultured with imDCs pulsed with 1µg/mL mutated or wild-type minimal peptides. **(C-D)** Highlighting known neoantigen-specific clones **(C)** and public viral-targeting clones **(E)** Phenotypic clustering of Pt.4317 tetramer-enriched circulating CD8+ PBLs. UMAP clusters from 4317 PBL-derived CD8+ T cells. **(F-G)** Cluster distribution of HLA A*02:01-restricted tetramer-sorted PIK3CA^{P449T} neoantigen T cells **(F)** and FluM1$_{(58-66)}$, EBV LMP2A$_{(426-434)}$ viral T cells **(G)** within PBL. **(H)** Transcriptome expression of top

genes expressed in cluster 11 (indicated by arrow) that harbors neoantigen-T cells**. (l)** Heatmap of antibody CITEseq-antibodies intensities on cells in scRNAseq clusters including Cluster 11 (indicated by arrow).

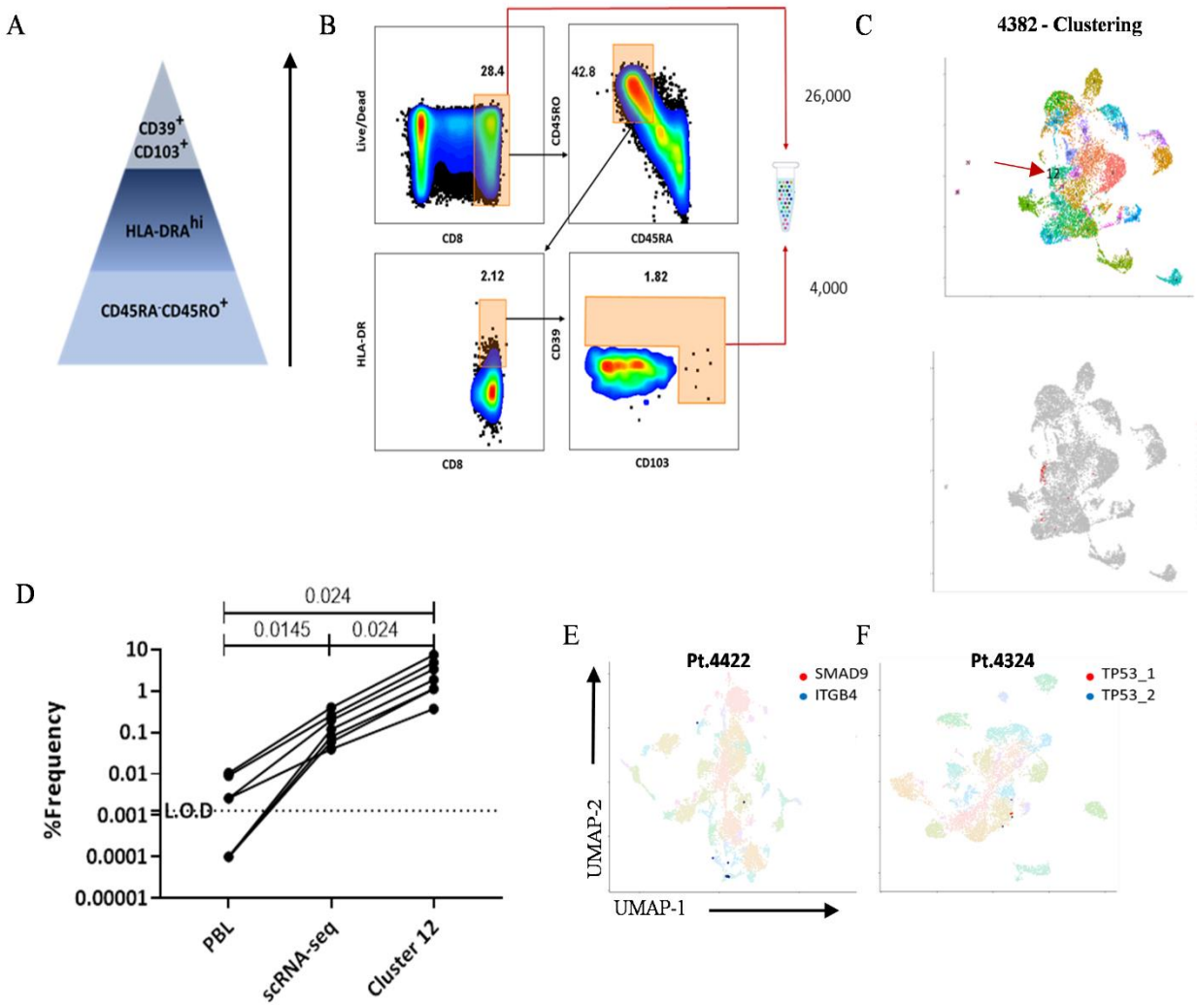

Supplemental Figure S3: Tetramer-agnostic circulating CD8⁺ PBL T cells by FACS-sorting strategy, related to Figure 1. (A) Sorting strategy used for the enrichment of circulating neoantigen-reactive CD8⁺ T cells in samples from patients 4382, 4422, and 4324. **(B-C)** Representative example of enrichment sorting **(B)** and scRNA analysis for pt.4382, Archival neoantigen-reactive cells are highlighted in red **(C)**. **(D)** Frequency of neoantigen-reactive T cell in PBL, sorted cells (scRNA-seq), and within cluster 12. Numbers in the graph represent p-value of paired T-test. **(E-F)** Projection of neoantigen-reactive T cell clones on UMAP space for pt.4422 **(E)** and pt.4324 **(F)**.

A

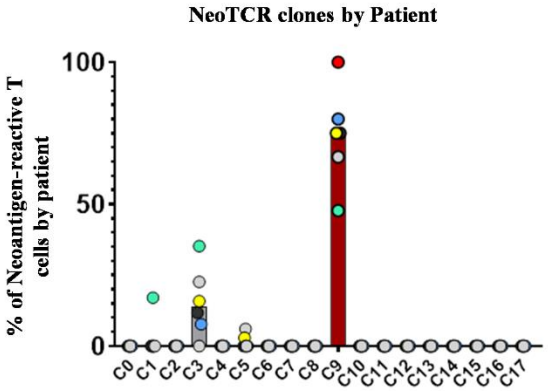
NeoTCR clones by Patient
% of Neoantigen-reactive T cells by patient
100
50
0
C0 C1 C2 C3 C4 C5 C6 C7 C8 C9 C10 C11 C12 C13 C14 C15 C16 C17

B

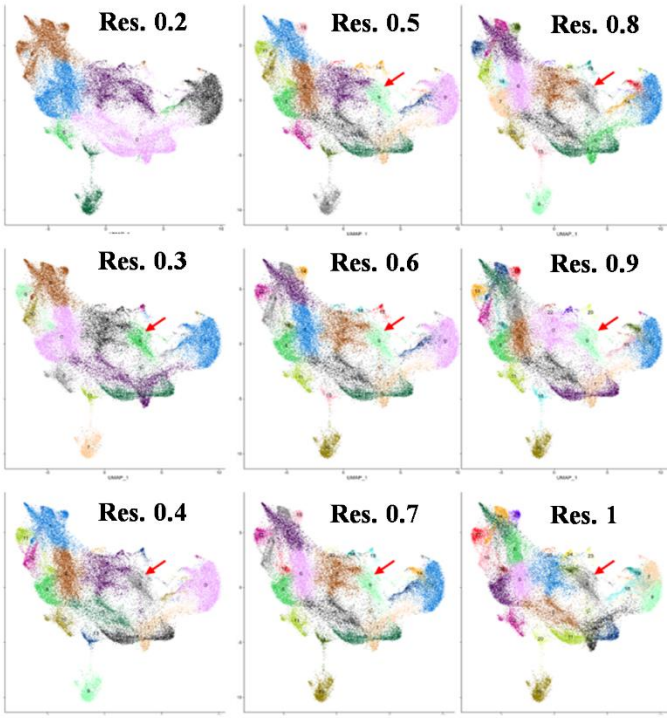
Res. 0.2
Res. 0.5
Res. 0.8
Res. 0.3
Res. 0.6
Res. 0.9
Res. 0.4
Res. 0.7
Res. 1

C

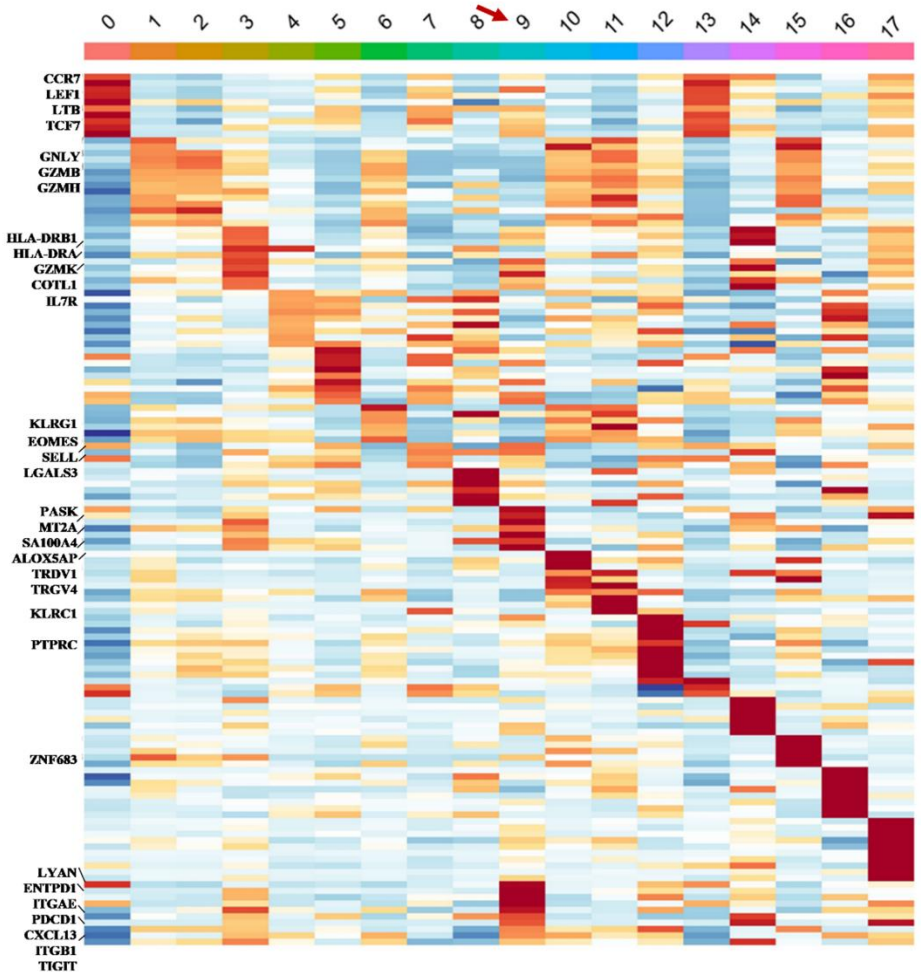
0 1 2 3 4 5 6 7 8 9 10 11 12 13 14 15 16 17
CCR7
LEF1
LTB
TCF7
GNLY
GZMB
GZMH
HLA-DRB1
HLA-DRA
GZMK
COTL1
IL7R
KLRG1
EOMES
SELL
LGALS3
PASK
MT2A
SA100A4
ALOX5AP
TRDV1
TRGV4
KLRC1
PTPRC
ZNF683
LYAN
ENTPD1
ITGAE
PDCD1
CXCL13
ITGB1
TIGIT

Supplemental Figure S4: Combined phenotype and frequency analysis of NeoTCRPBL clones from the 6 patients with neoantigen TIL-reactivity, related Figure 2. (A) $NeoTCR_{PBL}$ clones from each of the 6 patients are enriched within cluster 9. Each colored circle represents the total frequency of neoantigen-specific T cell clones from each of the 6 patients. **(B)** $NeoTCR_{PBL}$ transcriptomic state remains intact over a wide range of resolution parameters in the 6 patient PBL. Arrow indicates Cluster 9 shown in Figure 2. **(C)** Heatmap of differentially expressed genes and genes-of-interest across UMAP clusters shown in Figure 2 (derived from samples from 6 patients). Cluster 9 indicates $NeoTCR_{PBL}$ cluster. The last 10 rows indicate T cell dysfunction markers of interest.

A

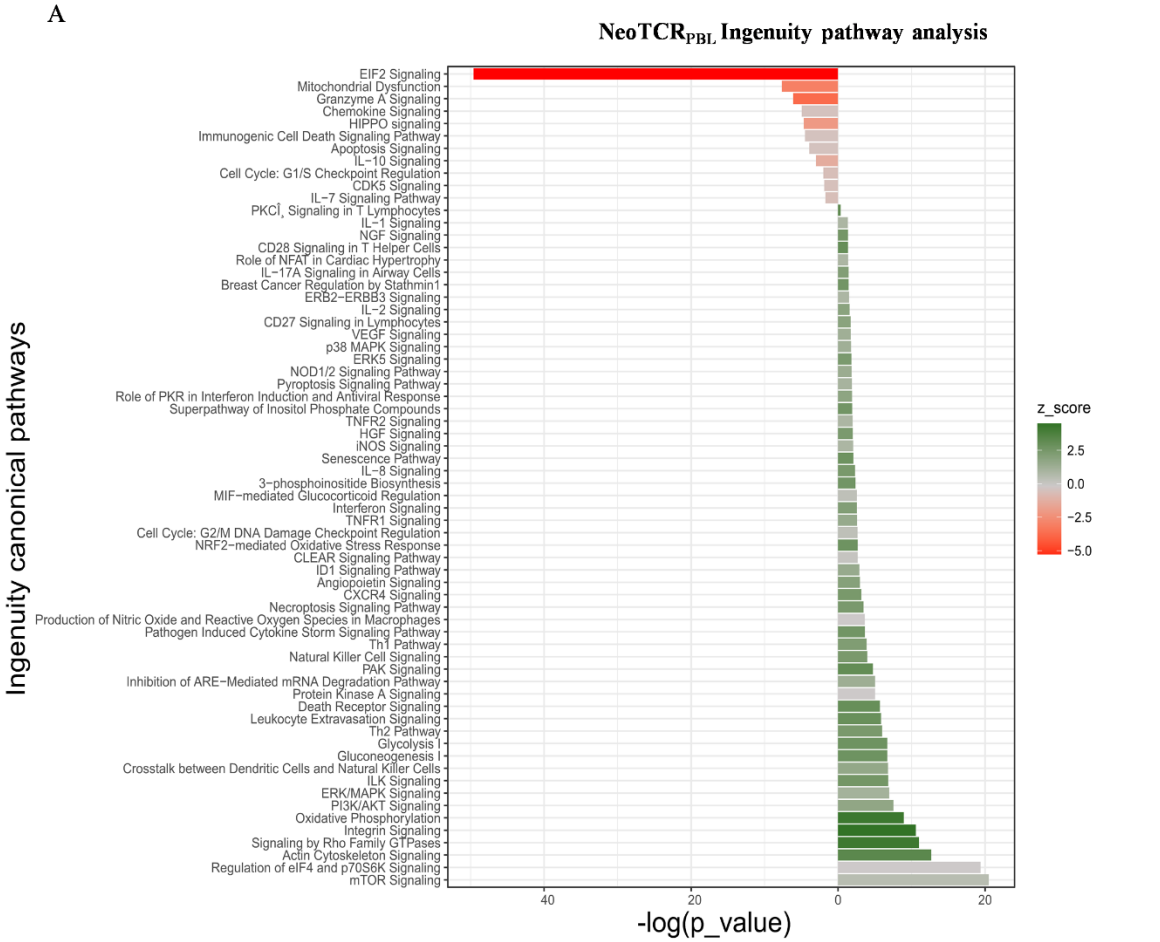
NeoTCR$_{PBL}$ Ingenuity pathway analysis
Ingenuity canonical pathways
EIF2 Signaling
Mitochondrial Dysfunction
Granzyme A Signaling
Chemokine Signaling
HIPPO signaling
Immunogenic Cell Death Signaling Pathway
Apoptosis Signaling
IL-10 Signaling
Cell Cycle: G1/S Checkpoint Regulation
CDK5 Signaling
IL-7 Signaling Pathway
PKCÎ¸ Signaling in T Lymphocytes
IL-1 Signaling
NGF Signaling
CD28 Signaling in T Helper Cells
Role of NFAT in Cardiac Hypertrophy
IL-17A Signaling in Airway Cells
Breast Cancer Regulation by Stathmin1
ERB2-ERBB3 Signaling
IL-2 Signaling
CD27 Signaling in Lymphocytes
VEGF Signaling
p38 MAPK Signaling
ERK5 Signaling
NOD1/2 Signaling Pathway
Pyroptosis Signaling Pathway
Role of PKR in Interferon Induction and Antiviral Response
Superpathway of Inositol Phosphate Compounds
TNFR2 Signaling
HGF Signaling
iNOS Signaling
Senescence Pathway
IL-8 Signaling
3-phosphoinositide Biosynthesis
MIF-mediated Glucocorticoid Regulation
Interferon Signaling
TNFR1 Signaling
Cell Cycle: G2/M DNA Damage Checkpoint Regulation
NRF2-mediated Oxidative Stress Response
CLEAR Signaling Pathway
ID1 Signaling Pathway
Angiopoietin Signaling
CXCR4 Signaling
Necroptosis Signaling Pathway
Production of Nitric Oxide and Reactive Oxygen Species in Macrophages
Pathogen Induced Cytokine Storm Signaling Pathway
Th1 Pathway
Natural Killer Cell Signaling
PAK Signaling
Inhibition of ARE-Mediated mRNA Degradation Pathway
Protein Kinase A Signaling
Death Receptor Signaling
Leukocyte Extravasation Signaling
Th2 Pathway
Glycolysis I
Gluconeogenesis I
Crosstalk between Dendritic Cells and Natural Killer Cells
ILK Signaling
ERK/MAPK Signaling
PI3K/AKT Signaling
Oxidative Phosphorylation
Integrin Signaling
Signaling by Rho Family GTPases
Actin Cytoskeleton Signaling
Regulation of eIF4 and p70S6K Signaling
mTOR Signaling
40
20
0
20
-log(p_value)
z_score
2.5
0.0
-2.5
-5.0

B

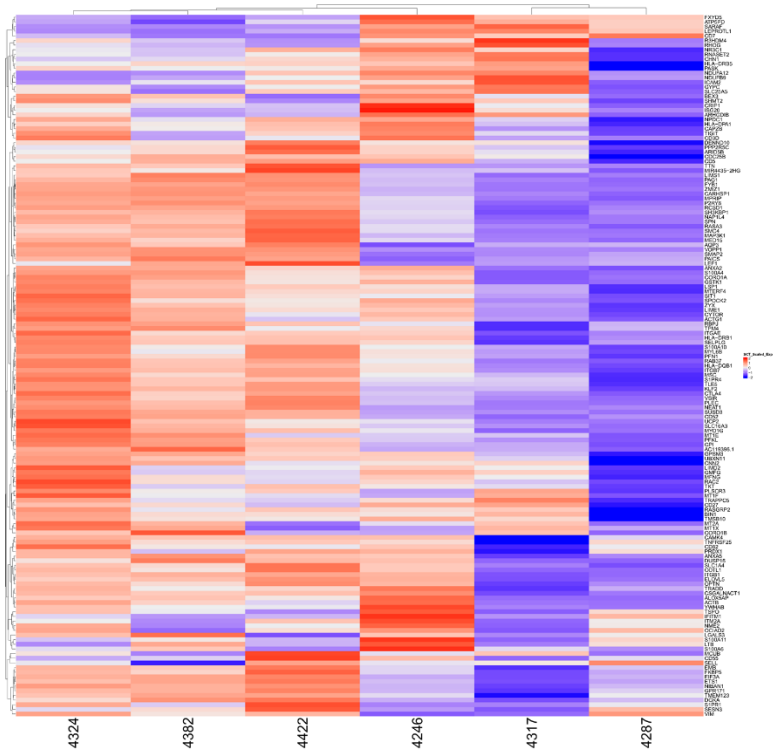
Gene expression variation by sample within Cluster 9
4324
4382
4422
4246
4317
4287

Supplemental Figure S5: Ingenuity pathway analysis (IPA) and gene expression sample variation of NeoTCR$_{PBL}$ gene signature, related to Figure 2. (A) Canonical pathway analysis showing activated (positive Z score) and inhibited (negative) pathways of the NeoTCR$_{PBL}$ gene signature. The X-axis indicates the significance of the enrichment. **(B)** Inter-patient variation of genes expressed within neoantigen-specific T cells found within cluster 9. Note that these comparisons are performed within cells from cluster 9 compared by each patient.

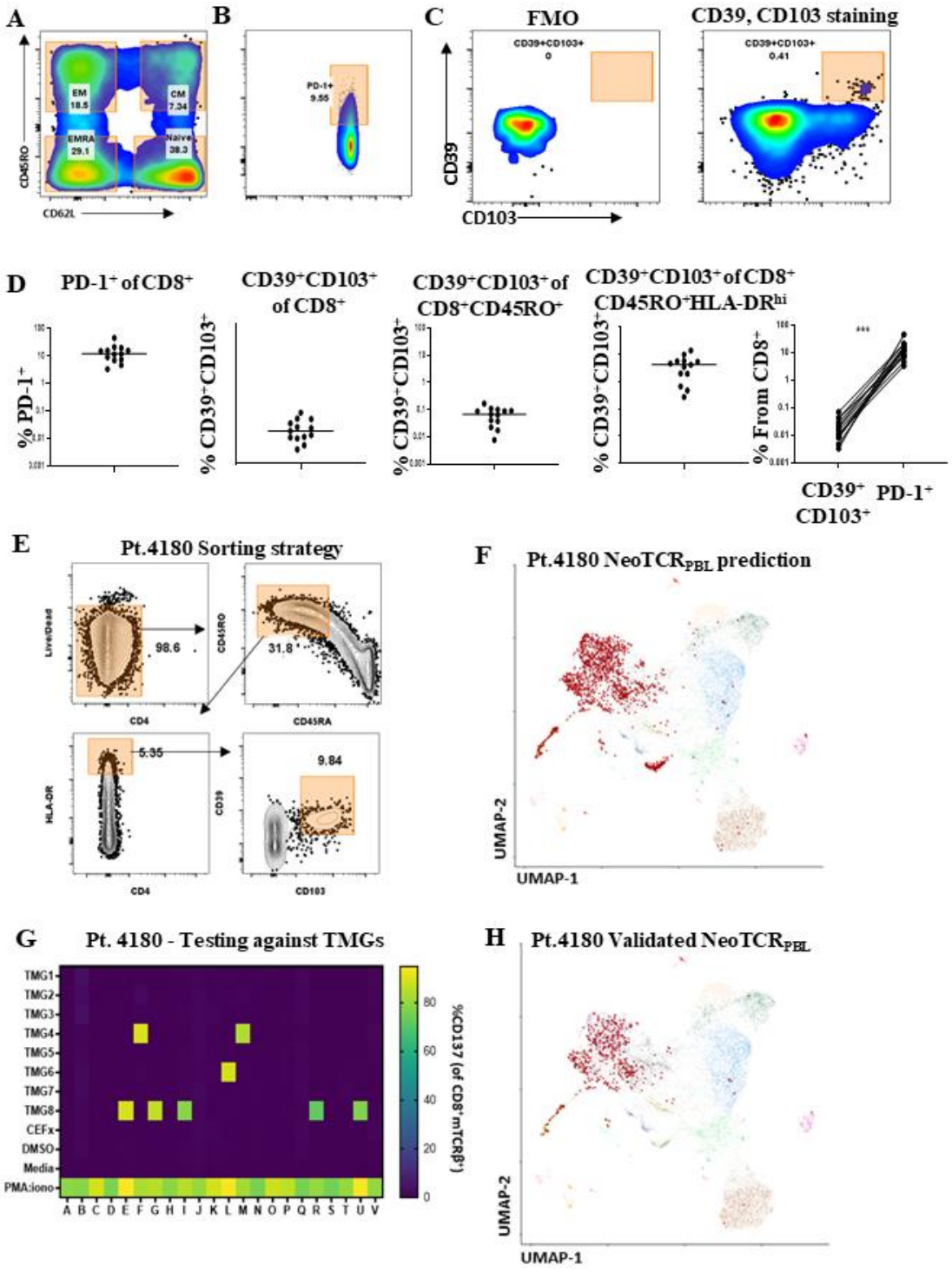

Supplemental Figure S6: Frequency of neoantigen-reactive T cells in PBL subsets (related to Figure 3A) and prospective prediction of NeoTCRs from PBL of breast cancer patient Pt.4180, related to Figure 3. (A-B) $CD8^+$ sorting gating strategy for naïve, memory **(A)**, and PD-1-expressing cells **(B)**. **(C)** CD39 and CD103 fluorescence-minus-one (FMO) and staining and sorting gates for $CD8^+$ T cells. **(D)** Frequency of FACS-sorted T cell subsets using

common cell surface markers previously used to identify antitumor T cells from $CD8^+$ PBL T cells within metastatic cancer patients **(E)** Prediction and functional validation of neoantigen-reactive TCRs for melanoma patient 4180. Sorting enrichment gating of circulating $CD8^+$ T cells for scRNAseq. 50,000 $CD39^+CD103^+$ were sorted and mixed with 100,000 bulk $CD8^+$ cells **(F)** UMAP unsupervised clustering and prediction of $NeoTCR_{PBL}$ based on scGSEA (in red). **(G)** Frequency of TCR-transduced $CD8^+$ cells expressing CD137 following co-culture with imDCs electroporated with patient's TMGs. **(H)** Back-projection identified neoantigen-reactive $NeoTCR_{PBL}$ clones onto the UMAP plot.

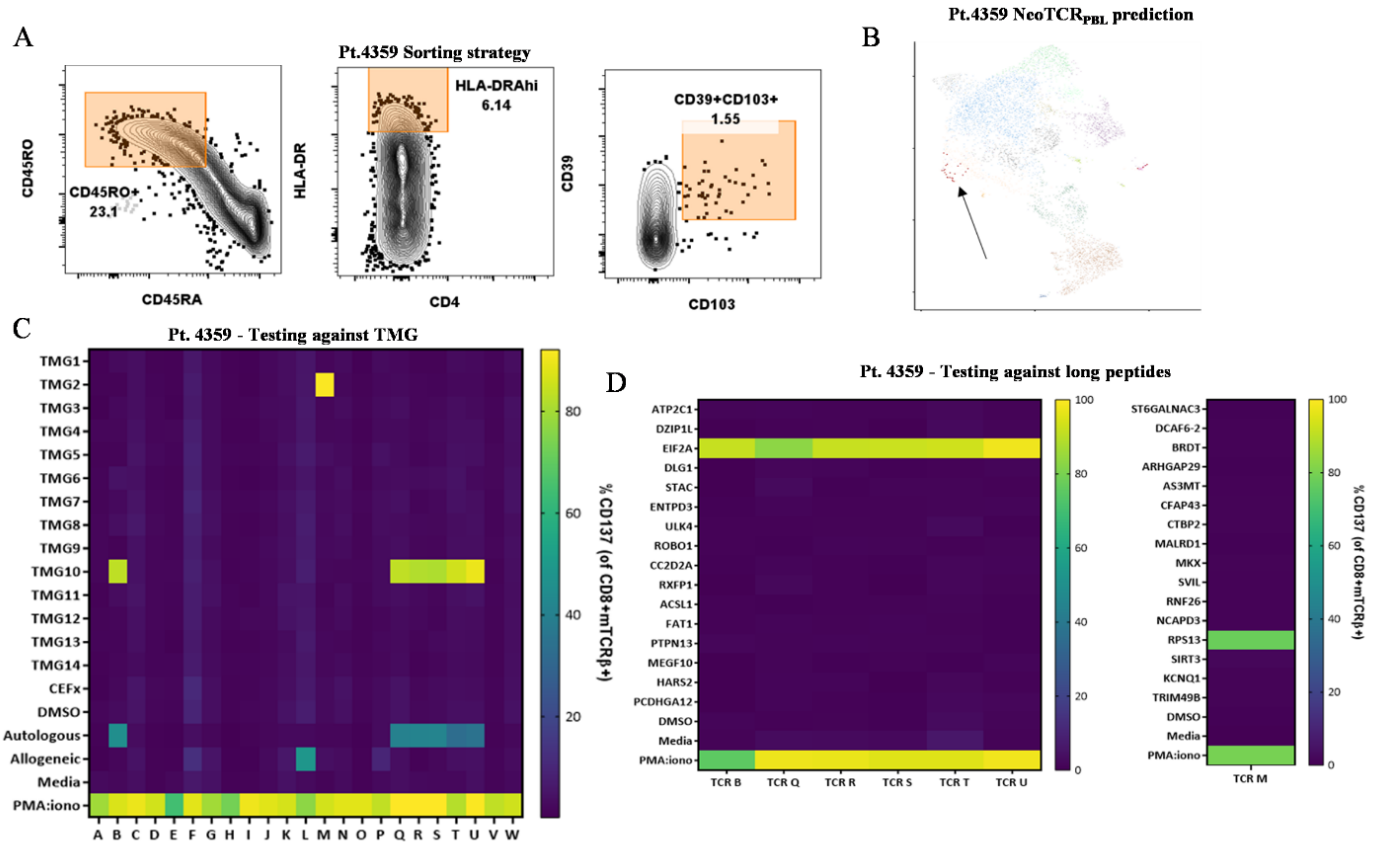

Supplemental Figure S7: Prediction and functional validation of neoantigen-reactive TCRs for melanoma patient 4359, related Figure 3. (A) Sorting enrichment gating of circulating CD8$^+$ T cells for scRNA. 6,800 CD39$^+$CD103$^+$ were sorted and mixed with 20,000 bulk CD8$^+$ cells **(B)** UMAP unsupervised clustering and prediction of NeoTCR$_{PBL}$ based on scGSEA (in red) **(C-D)** Frequency of TCR-transduced CD8$^+$ cells expressing CD137 following co-culture with imDCs electroporated with patient's TMGs **(C)** or peptides of TMG2 and 10 **(D)**.

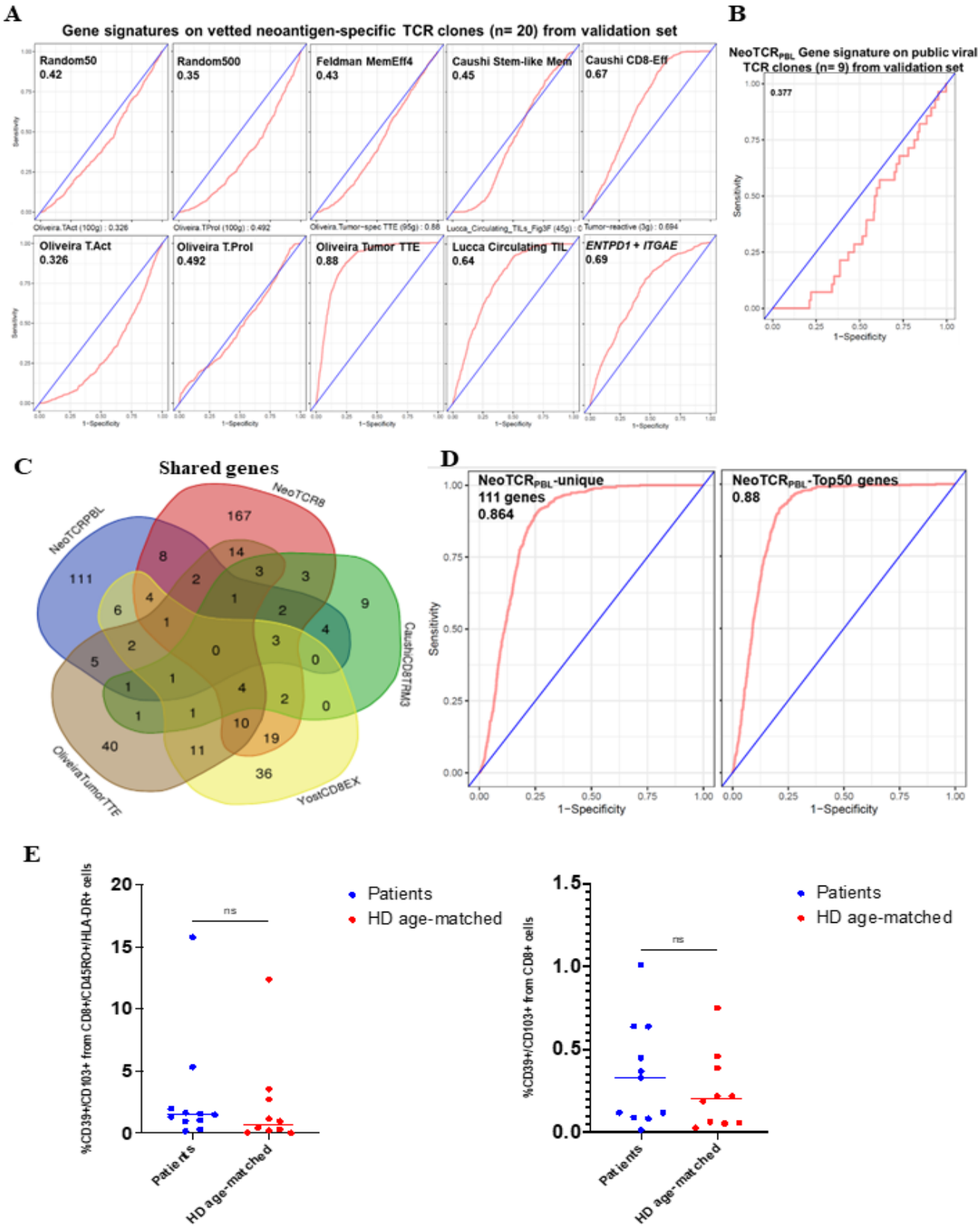
A
Gene signatures on vetted neoantigen-specific TCR clones (n= 20) from validation set
Random50
0.42
Random500
0.35
Feldman MemEff4
0.43
Caushi Stem-like Mem
0.45
Caushi CD8-Eff
0.67
Oliveira T.Act
0.326
Oliveira T.Prol
0.492
Oliveira Tumor TTE
0.88
Lucca Circulating TIL
0.64
ENTPD1 + ITGAE
0.69
Sensitivity
1−Specificity
B
NeoTCR$_{PBL}$ Gene signature on public viral TCR clones (n= 9) from validation set
0.377
Sensitivity
1−Specificity
C
Shared genes
NeoTCR8
NeoTCRPBL
OliveiraTumorTTE
YostCD8EX
CaushCD8TRM3
167
111
40
36
9
8
14
3
3
2
1
4
6
1
2
0
5
1
1
4
2
0
1
1
10
19
11
D
NeoTCR$_{PBL}$-unique
111 genes
0.864
NeoTCR$_{PBL}$-Top50 genes
0.88
Sensitivity
1−Specificity
E
%CD39+/CD103+ from CD8+/CD45RO+/HLA-DR+ cells
ns
Patients
HD age-matched
%CD39+/CD103+ from CD8+ cells
ns
Patients
HD age-matched

Supplemental Figure S8: Sensitivity and Specificity of gene signatures in predicting TCR clonotypes from the validation set, and frequency of NeoTCR$_{PBL}$ CD8+ T cells in healthy donors, related Figure 3. (A) NeoTCR$_{PBL}$ clone prediction by gene signatures **(B)** NeoTCR$_{PBL}$ gene signature has poor sensitivity in predicting public viral clonotypes (n = 9) from the validation set. **(C)** Overlap of NeoTCR$_{PBL}$ signature with other antitumor TIL programs. Venn diagram of shared genes between the 4 tumor-relevant TIL signatures and NeoTCR$_{PBL}$. **(D)** Neoantigen-specific T clone prediction performance of the 111 unique genes from NeoTCR$_{PBL}$ (left panel) and the top 50 NeoTCR$_{PBL}$ genes (right panel). **(E)** CD39^{+}CD103^{+} CD8 T cells frequency in peripheral blood of patients with metastatic cancer and age-matched healthy donors. Frequency in CD45RO^{+}HLA-DR^{+} (left panel) and bulk CD8^{+} (right panel).